

Supplementary Material

Fe, S-uniformly dispersed Ni MOFs based on FeS substrate precipitation-dissolution equilibrium for water and seawater oxidation

Na Xu, Fu-Li Wang, Jun-Qi Han, Wen-Li Yu, Wen-Jing Li, Yi-Chuan Li, Yu-Lu Zhou,

Yong-Ming Chai *, Bin Dong*

State Key Laboratory of Heavy Oil Processing, College of Chemistry and Chemical Engineering,

China University of Petroleum (East China), Qingdao 266580, PR China

* Corresponding author. Email: ymchai@upc.edu.cn(Y.M. Chai); dongbin@upc.edu.cn (B. Dong)

Tel: +86-532-86981156, Fax: +86-532-86981156

Experimental section

Anhydrous ethanol (≥ 99.7 wt.%) was purchased from Shanghai Titan Scientific Co. Ltd., China. Nickel foam (thickness: 1.5 mm) and iron foam (thickness: 1.5 mm) were bought from Kunshan Lvchuang Electronic Technology Co. Ltd., China. Sodium sulfate decahydrate $\text{Na}_2\text{S}\cdot 9\text{H}_2\text{O}$ (≥ 99.0 wt.%), nickel nitrate hexahydrate $\text{Ni}(\text{NO}_3)_2\cdot 6\text{H}_2\text{O}$ (≥ 98.5 wt.%), potassium hydroxide KOH (≥ 85.0 wt.%), potassium hydroxide KOH (≥ 85.0 wt.%) and *N,N'*-Dimethylformamide (DMF) ($\geq 99.5.0$ wt.%) were purchased from Sinopharm Chemical Reagent Co. Ltd., China. Terephthalic acid (≥ 99.0 wt.%) was bought from Shanghai Macklin Biochemical Co. Ltd., China. All the experimental chemicals and materials used were of analytical purity and no further post-treatment was required before use.

Materials characterization

The structure and compositions of the samples were examined by SEM (Quanta FEG 450, 20.0 kV) and TEM (TALOS F200X). High-resolution transmission electron microscopic (HRTEM) images were taken on FEI Tecnai G20. The X-ray diffraction (XRD, Bruker D8) data were recorded by means of $\text{Cu } K_\alpha$ with 2θ range from 20° to 85° . Energy dispersive X-ray spectroscopy (EDX) is characterized on the Hitachi S-4800 to obtain the element composition and distribution of the resulting sample. XPS analysis was recorded by Thermo Fisher Scientific. The Fourier transform infrared (FT-IR) spectra were performed with IR Tracer-100.

Electrochemical measurements

The electrochemical measurements were carried out in a variety of electrolytes, including alkaline seawater (1 M KOH saltwater), using a typical three-electrode cell setup at ambient

temperature. During all tests, the saturated calomel electrode (SCE) and Pt wire served as the reference electrode and counter electrode, respectively. Linear sweep voltammograms (LSVs) measurements were conducted under a scanning rate of 5 mV s^{-1} with iR-compensation. The end overpotentials were obtained through $E(\text{RHE}) = E(\text{SCE}) + 0.243 \text{ V} + 0.059 \text{ pH}$. Using a frequency range of 100 kHz to 0.1 Hz, EIS Nyquist plots of the as-synthesized samples were measured. In an equivalent electrical circuit, R_s (R_1) stands for solution resistance, CPE for constant phase element and R_{ct} (R_2) for charge transfer resistance. Stability tests of chronopotentiometry measurements were carried out to evaluate the durability of prepared catalysts in electrolytes including 1M KOH and alkaline seawater (1M KOH seawater). To maintain objectivity, all measurements on reference samples were performed under identical conditions and according to the same measurement procedures, at room temperature.

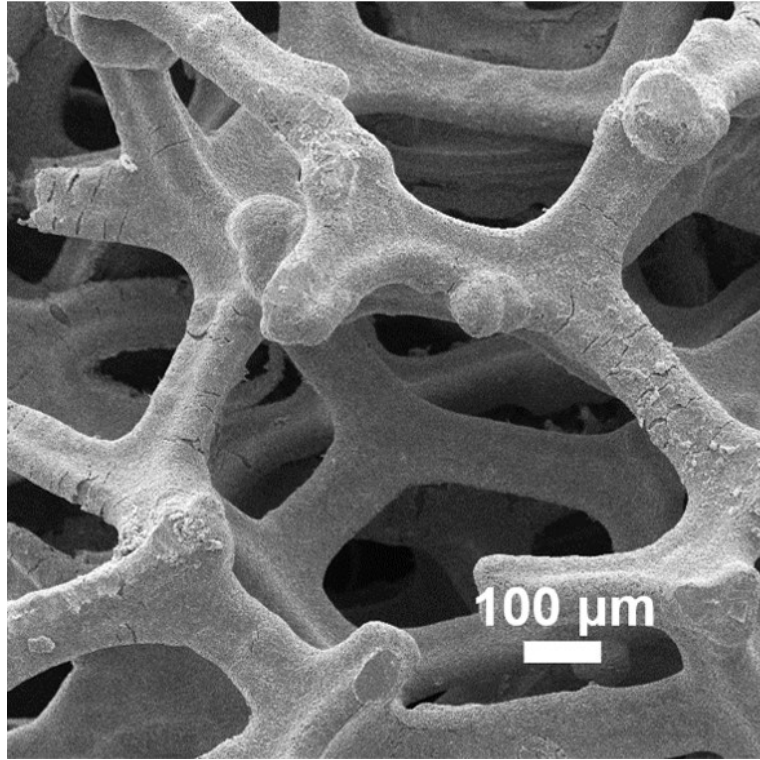


Fig. S1 SEM image of IF.

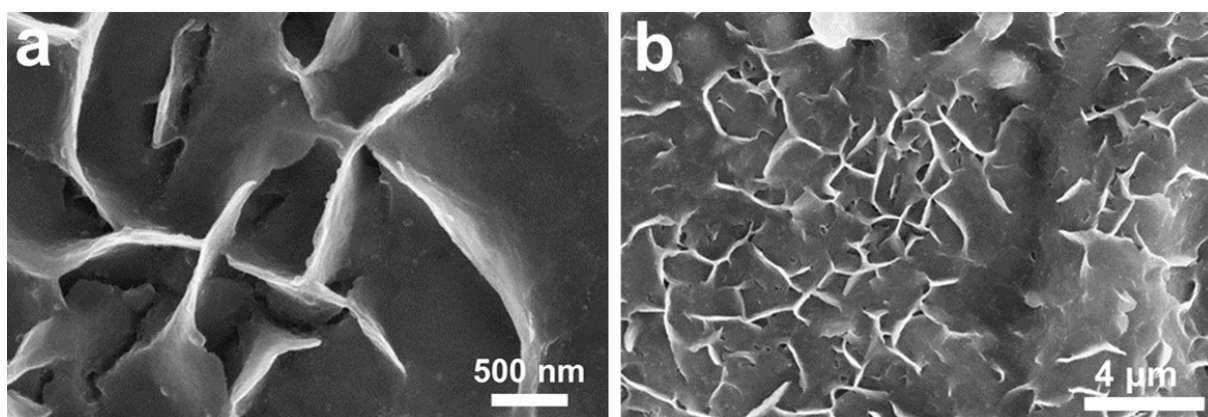


Fig. S2 Morphological characterization of (a-b) FeS/IF.

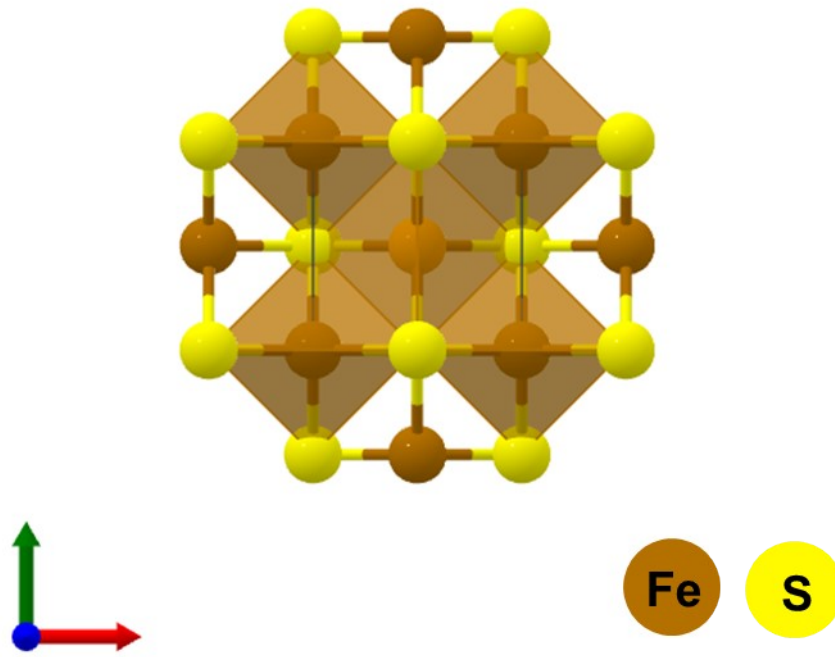


Fig. S3 The crystalline structure of mackinawite FeS.

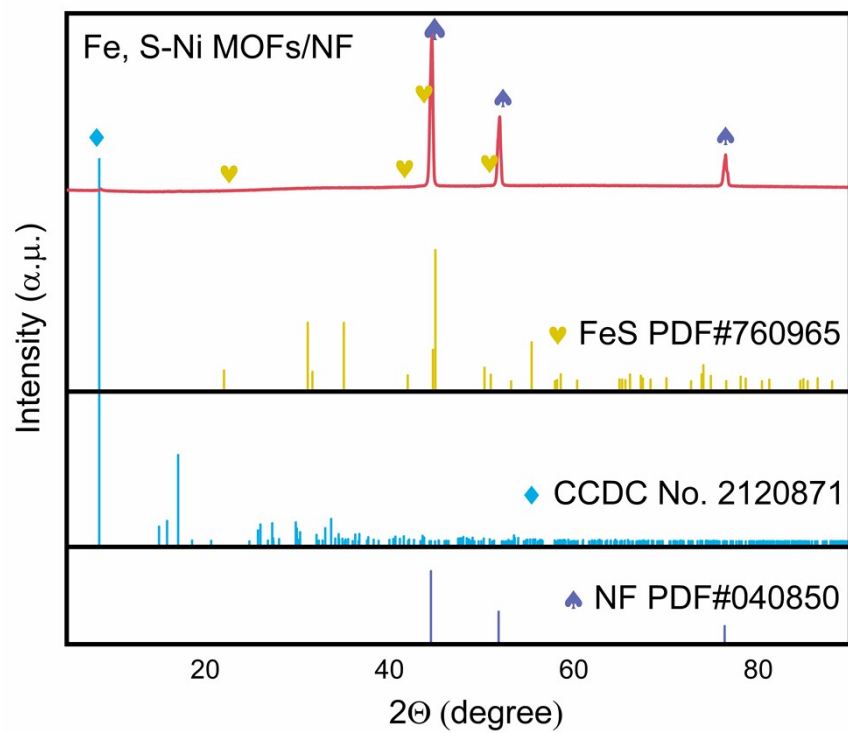


Fig. S4 XRD patterns of Fe, S-Ni MOFs/NF.

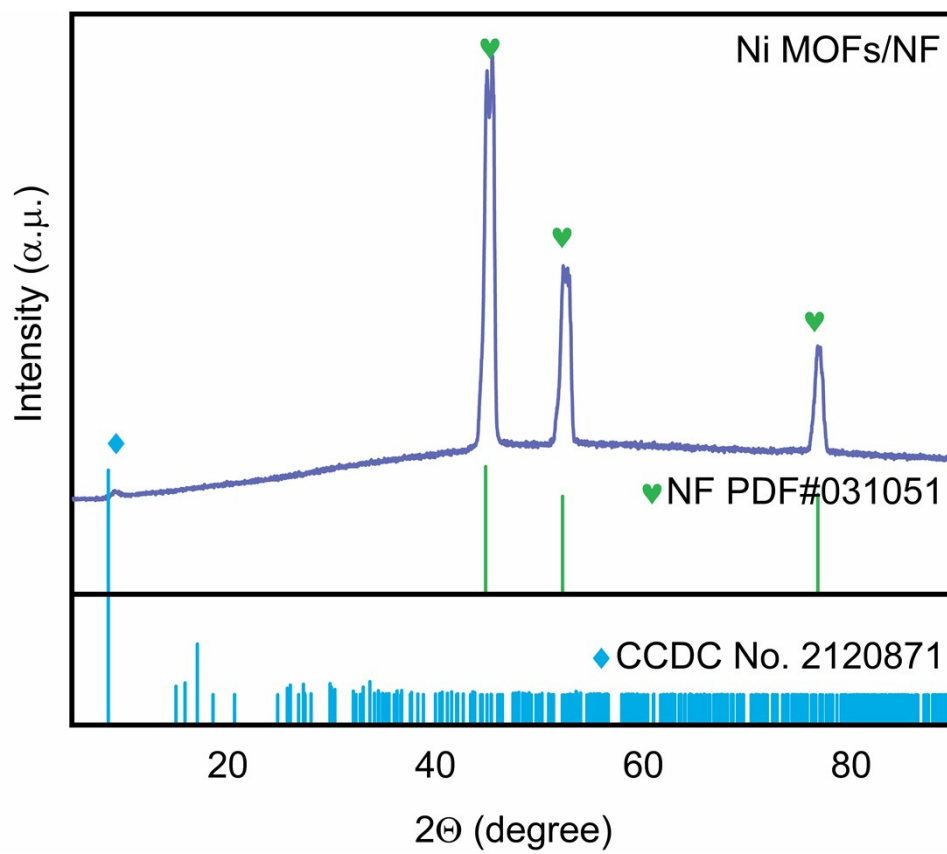


Fig. S5 XRD patterns of Ni MOFs/NF.

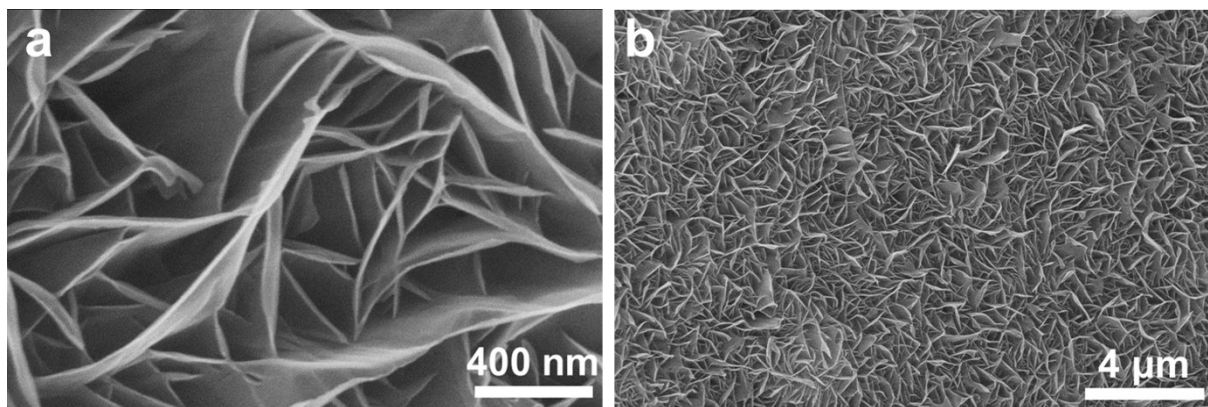


Fig. S6 SEM images of (a-b) Ni MOFs/NF sample.

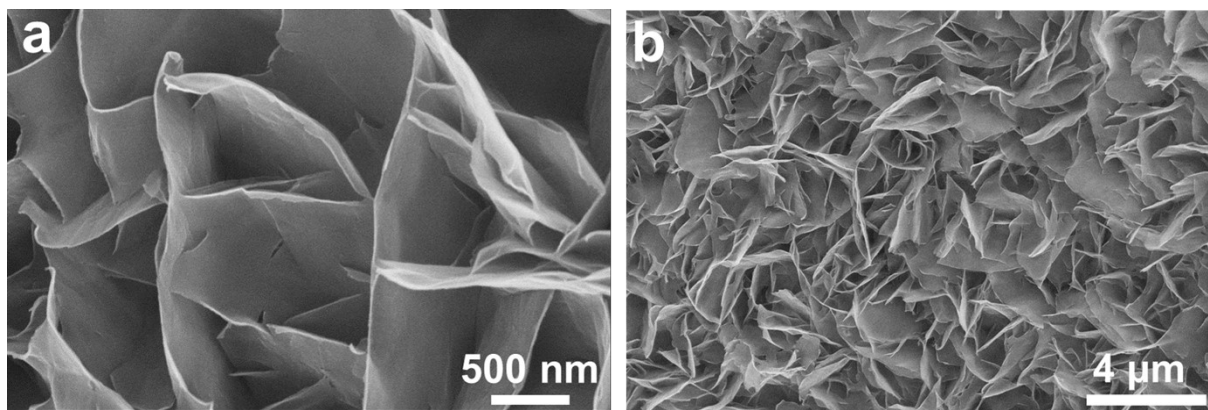


Fig. S7 SEM images of (a-b) Fe, S-Ni MOFs/NF sample.

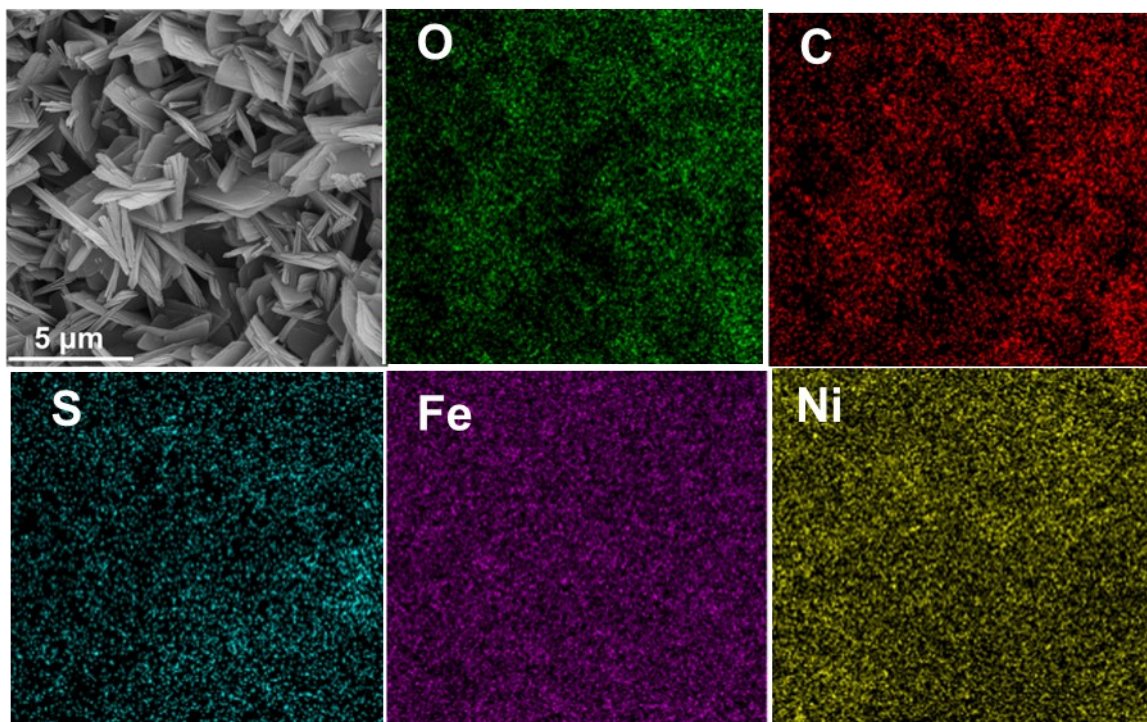


Fig. S8 SEM image and the corresponding elemental mappings of the Ni MOFs/FeS/IF.

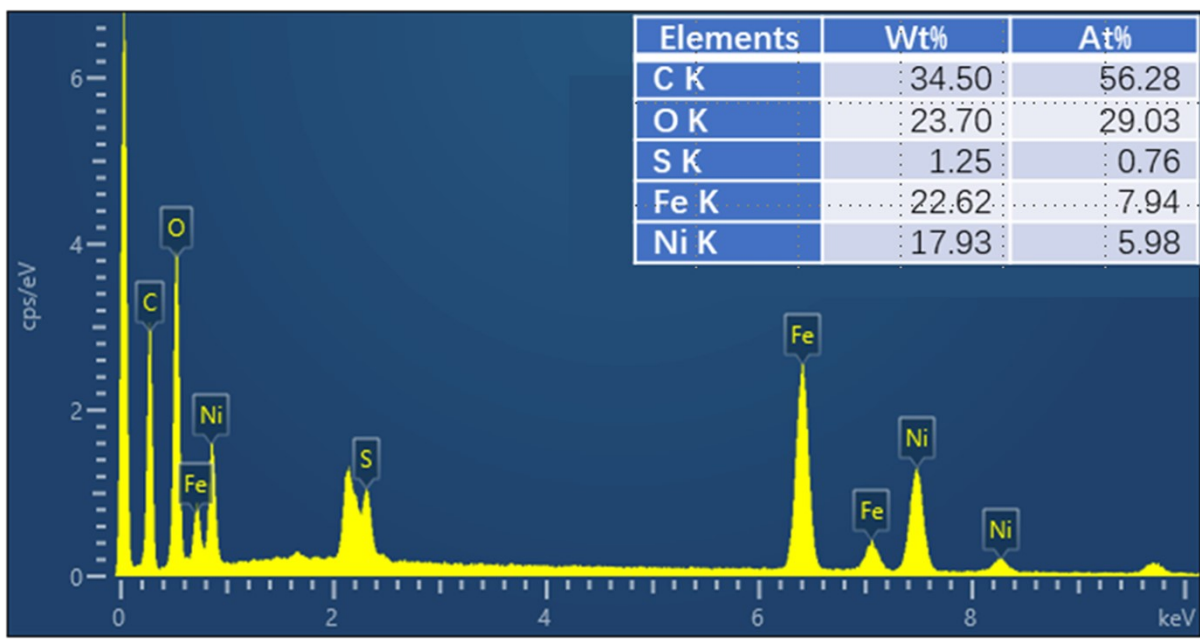


Fig. S9 EDS results of Ni MOFs/FeS/IF and corresponding element contents.

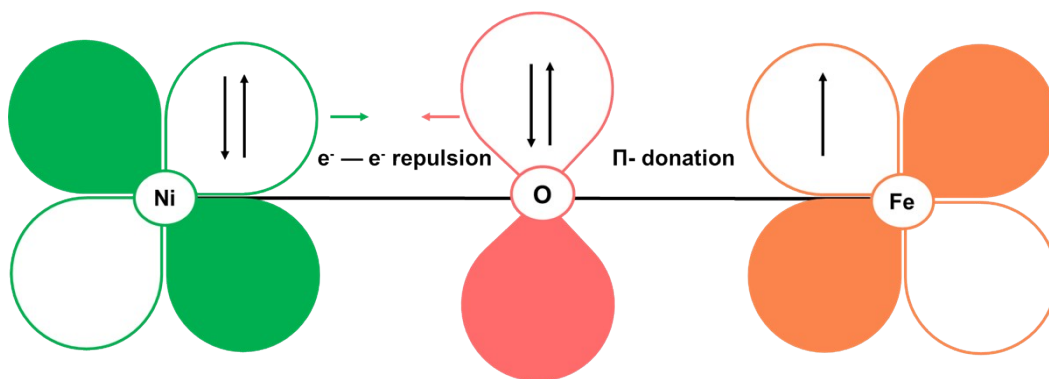


Fig. S10 Schematic representations of the electronic coupling of Ni-O-Fe [1].

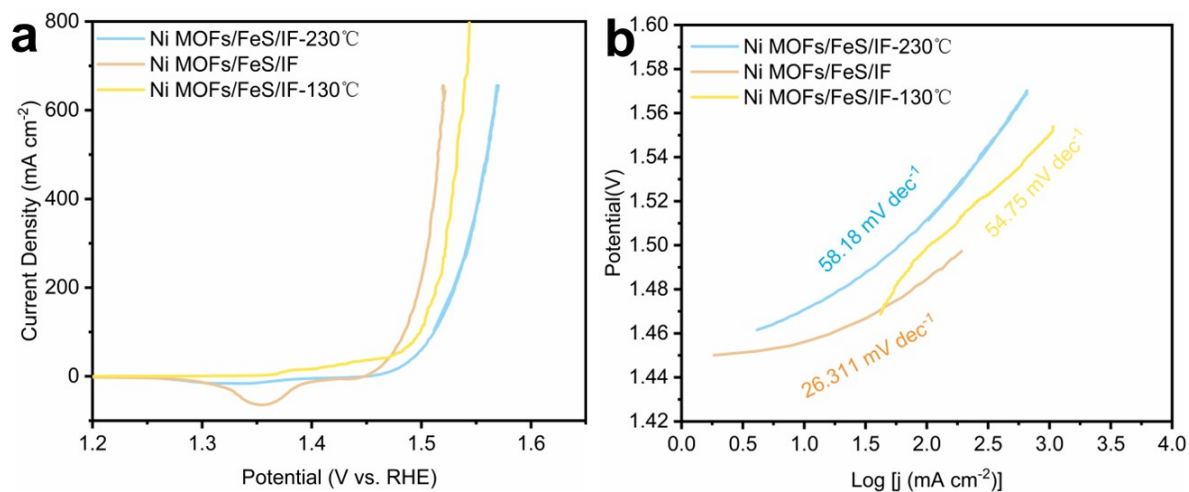


Fig. S11 (a) The polarization curves recorded on Ni MOFs/FeS/IF under alkaline media with different temperature. (b) The corresponding Tafel plots.

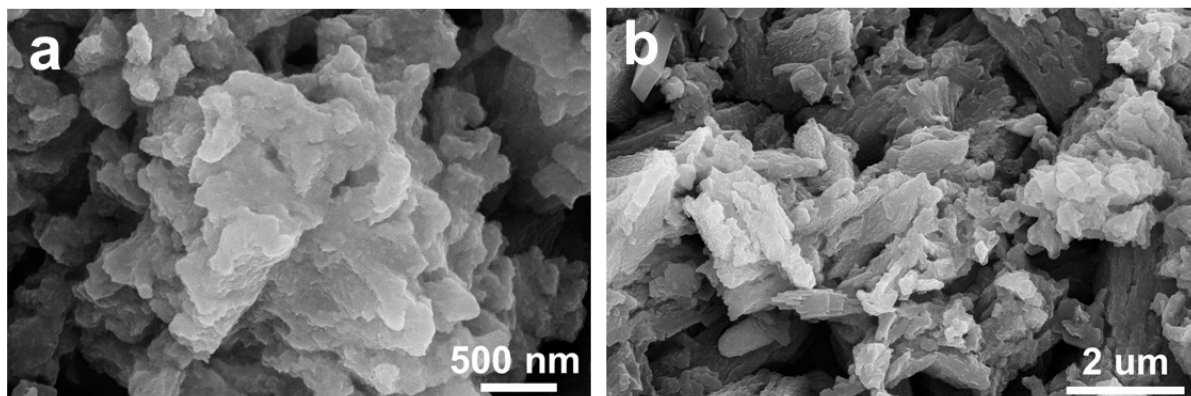


Fig. S12 SEM images of Ni MOFs/FeS/IF samples after long-term stability measurements in 1 M KOH.

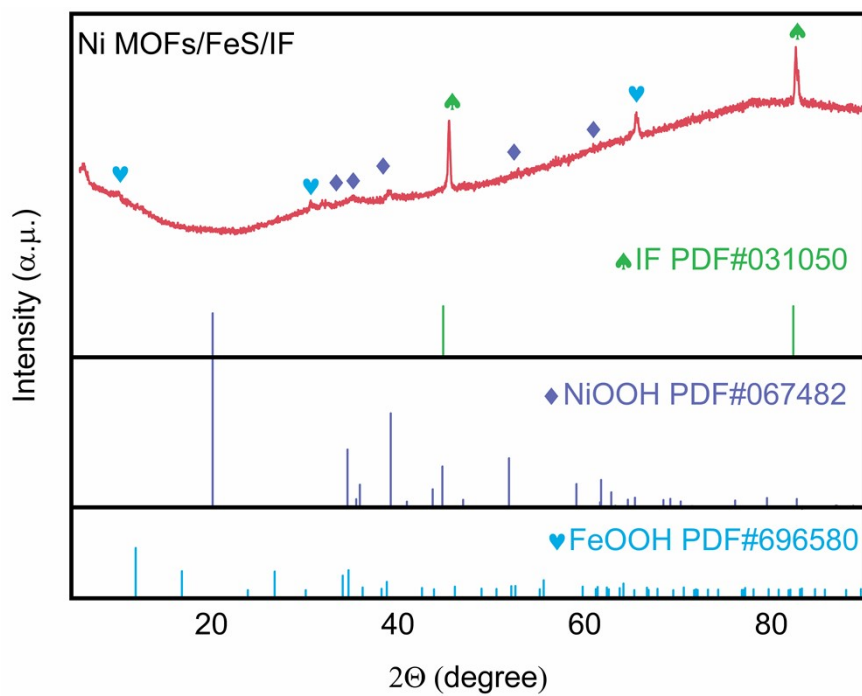


Fig. S13 XRD patterns of Ni MOFs/FeS/IF after long-term stability measurements in 1 M KOH.

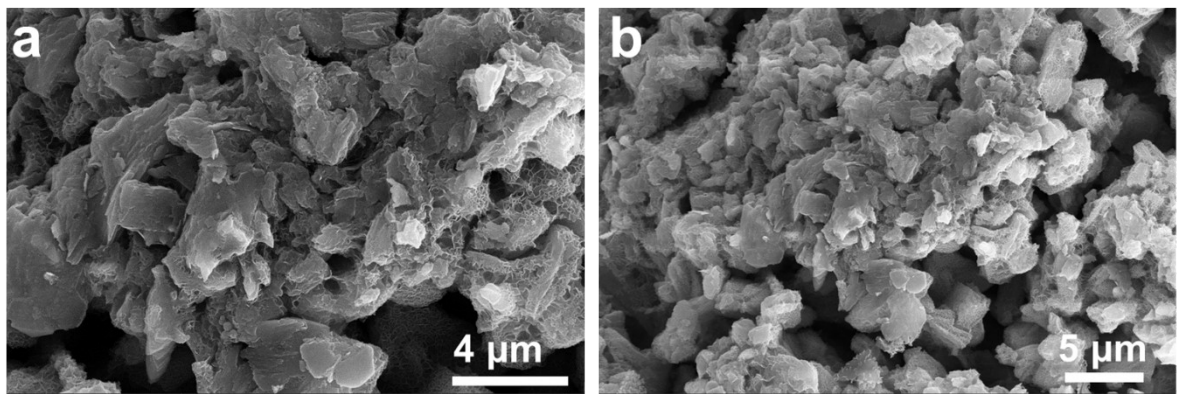


Fig. S14 SEM images of Ni MOFs/FeS/IF samples after OER measurements in 1 M KOH seawater.

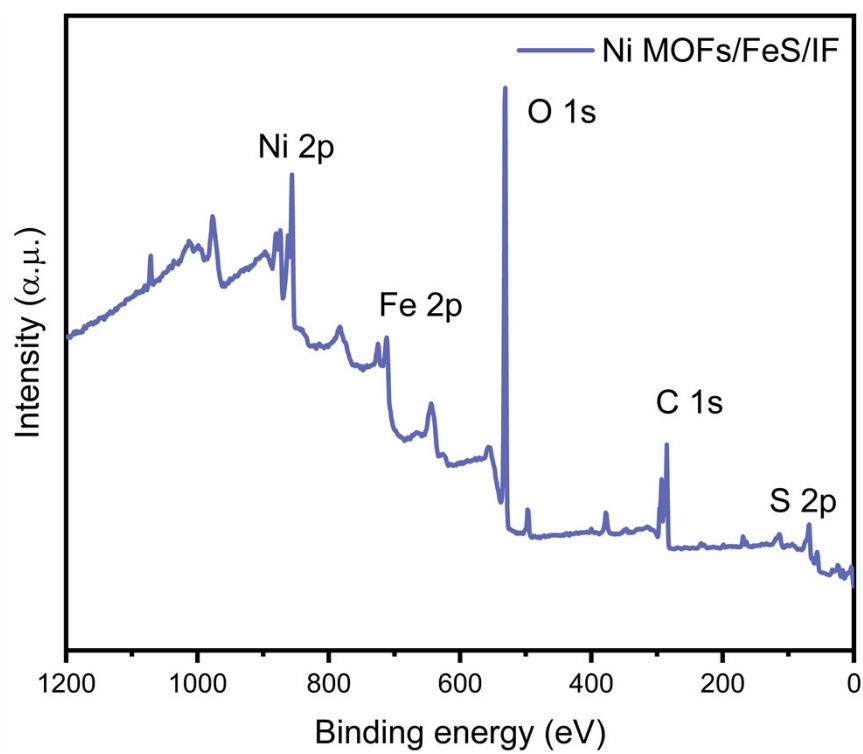


Fig. S15 (a) Survey XPS spectrum and high-resolution XPS spectra of Ni MOFs/FeS/IF electrode after OER in 1 M KOH seawater.

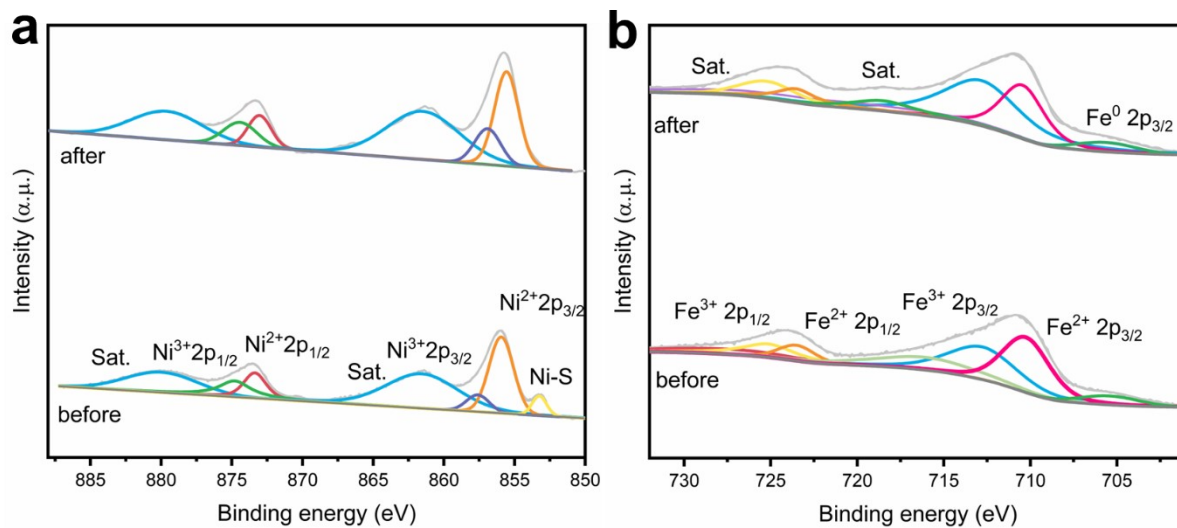


Fig. S16 High-resolution XPS spectra at (a) Ni 2p and (b) Fe 2p and regions of Ni MOFs/FeS/IF electrode before and after OER in 1 M KOH seawater.

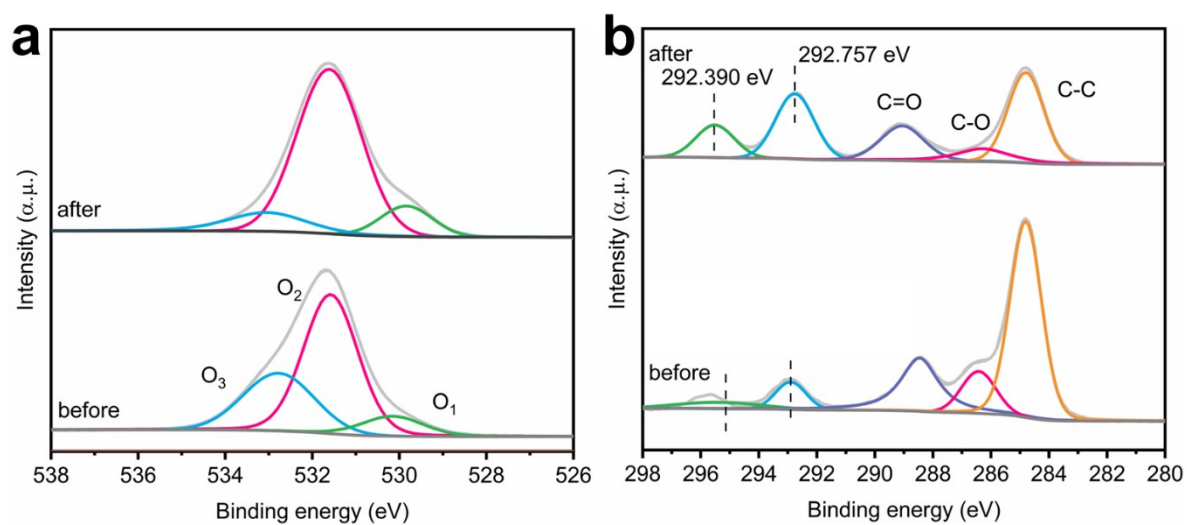


Fig. S17 High-resolution XPS spectra at (a) O 1s and (b) C 1s of Ni MOFs/FeS/IF electrode before and after OER in 1 M KOH seawater.

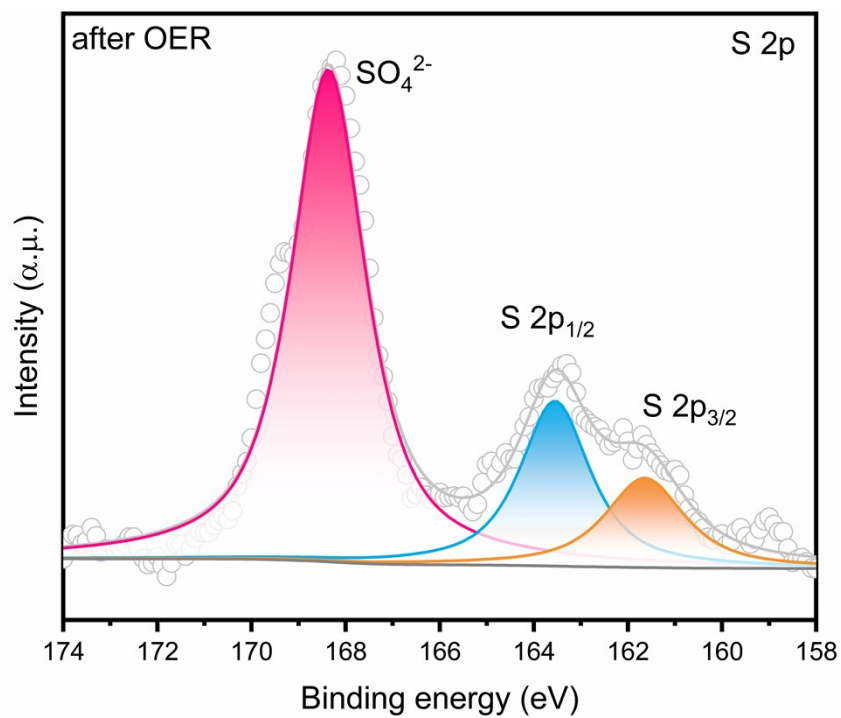


Fig. S18 high-resolution XPS spectra at S 2p regions of Ni MOFs/FeS/IF electrode after OER in 1 M KOH seawater.

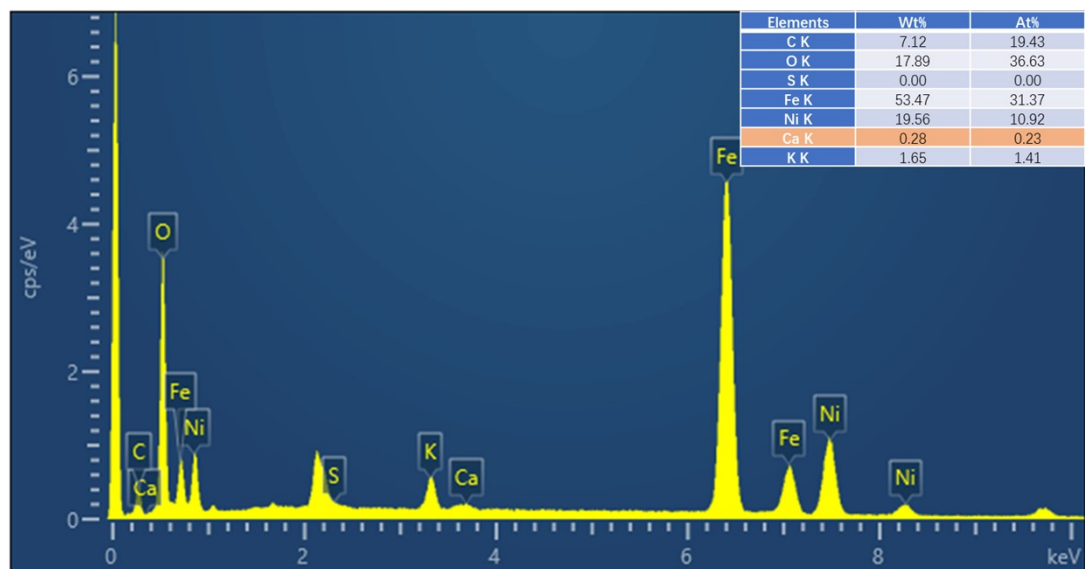


Fig. S19 EDS results of Ni MOFs/FeS/IF and corresponding element contents after OER test in 1M KOH seawater.

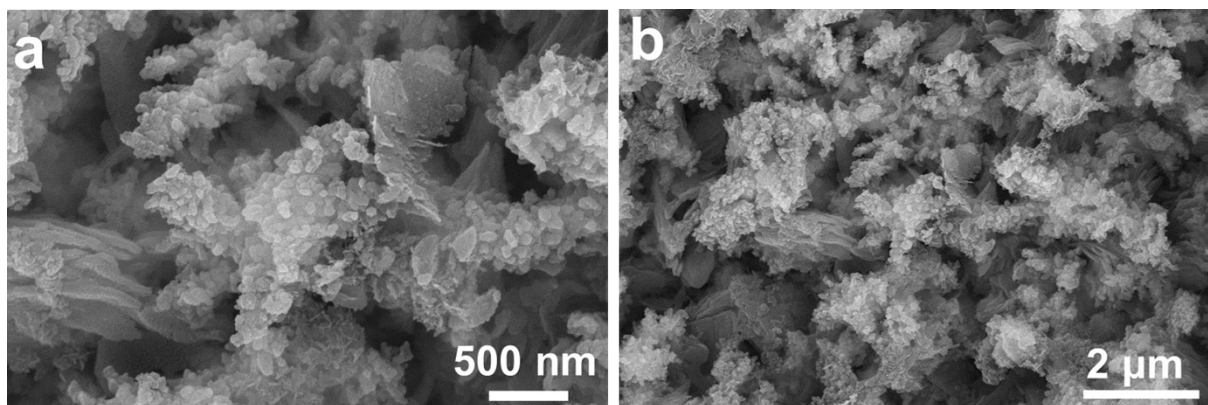


Fig. S20 SEM images of Ni MOFs/FeS/IF samples after long-term stability measurements in 1 M KOH seawater.

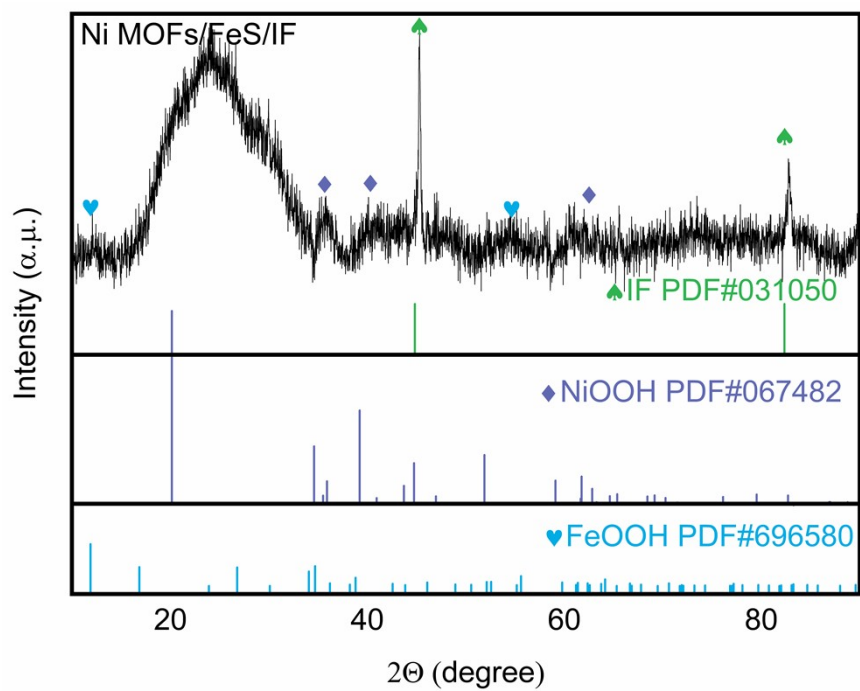


Fig. S21 XRD patterns of Ni MOFs/FeS/IF after OER measurements in 1 M KOH seawater.

Table S1 Comparison of OER performance of Ni MOFs/FeS/IF with other reported catalysts in 1M KOH.

Catalysts	j (mA cm ⁻²)	η (mV)	iR- correction	Refer.
Ni MOFs/FeS/IF	100	254	√	This work
NiFe-MOF/NF	100	300	×	[2]
NiFe LDH@NiCoP	100	350	×	[3]
NiCo-BDC	100	292	√	[4]
Ni ₃ S ₂ @NGCLs	100	370	√	[5]
MIL-53(Co-Ni)	100	262	√	[6]
NiV-MOF	100	290	√	[7]
Ni-MOF	100	310	√	[8]
(Ni ₂ Co ₁) _{0.925} Fe _{0.075} -MOF	100	300	√	[9]

Most of the reports adopted the iR-corrected data for estimating the overpotential under different current densities. Compared with the polarization curves without iR-correction, the deviation of the curves with iR-correction increases exponentially as the current density rises. In other words, the overpotential under high current densities obtained from iR-correction is meaningless.

Table S2 Comparison of OER performance of Ni MOFs/FeS/IF with other electrocatalysts in alkaline seawater (1 M KOH seawater).

Catalysts	j (mA cm ⁻²)	η (mV)	b (mV dec ⁻¹)	Refer.
Ni MOFs/FeS/IF	100	280	54.96	This work
Cr-Co _x P	100	334	79.2	[10]
NiCoS	100	360	42	[11]
1D-Cu@Co-CoO/Rh	100	400	52.4	[12]
Gd-CoB/Au	100	~315	42	[13]
FeP ₂ /NF	100	~315	56	[14]
Cu@CoFe LDH	100	300	44.4	[15]
Co-NC/CF	100	320	72	[16]
Ni ₅ Co ₃ Mo-H/NF	100	304	80	[17]

Reference

- [1] C. Ni, H. Zheng, W. Liu, L. Wu, R. Li, K. Zhou K and W. Zhang, Linker Defects in Metal–Organic Frameworks for the Construction of Interfacial Dual Metal Sites with High Oxygen Evolution Activity, *Adv. Funct. Mater.*, 2023:2301075.
- [2] J. Duan, S. Chen and C. Zhao, Ultrathin metal-organic framework array for efficient electrocatalytic water splitting, *Nat. Commun.*, 2017, **8**, 15341.
- [3] H. Zhang, X. Li, A. Hähnel, V. Naumann, C. Lin, S. Azimi, S. L. Schweizer, A. W. Maijenburg and R. B. Wehrspohn, Bifunctional Heterostructure Assembly of NiFe LDH Nanosheets on NiCoP Nanowires for Highly Efficient and Stable Overall Water Splitting, *Adv. Funct. Mater.*, 2018, **28**, 1706847.
- [4] B. Wang, J. Shang, C. Guo, J. Zhang, F. Zhu, A. Han, and J. Liu, A General Method to Ultrathin Bimetal-MOF Nanosheets Arrays via In Situ Transformation of Layered Double Hydroxides Arrays, *Small*, 2019, **15**, 1804761.
- [5] B. Li, Z. Li, Q. Pang and J. Zhang, Core/shell cable-like Ni₃S₂ nanowires/N-doped graphene-like carbon layers as composite electrocatalyst for overall electrocatalytic water splitting, *Chem. Eng. J.*, 2020, **401**, 126045.
- [6] M. Xie, Y. Ma, D. Lin, C. Xu, F. Xie and W. Zeng, Bimetal–organic framework MIL-53(Co–Fe): an efficient and robust electrocatalyst for the oxygen evolution reaction, *Nanoscale*, 2020, **12**, 67-71.
- [7] X. Sun, X. Zhang, Y. Li, Y. Xu, H. Su, W. Che, J. He, H. Zhang, M. Liu, W. Zhou, W. Cheng and Q. Liu, In Situ Construction of Flexible V□Ni Redox Centers over Ni-Based MOF Nanosheet Arrays for Electrochemical Water Oxidation, *Small Methods*, 2021, **5**,

2100573.

- [8] C. Meng, Y. Cao, Y. Luo, F. Zhang, Q. Kong, A. A. Alshehri, K. A. Alzahrani, T. Li, Q. Liu and X. Sun, A Ni-MOF nanosheet array for efficient oxygen evolution electrocatalysis in alkaline media, *Inorg. Chem. Front.*, 2021, **8**, 3007-3011.
- [9] Q. Qian, Y. Li, Y. Liu, L. Yu and G. Zhang, Ambient Fast Synthesis and Active Sites Deciphering of Hierarchical Foam-Like Trimetal–Organic Framework Nanostructures as a Platform for Highly Efficient Oxygen Evolution Electrocatalysis, *Adv. Mater.*, 2019, **31**, 1901139.
- [10] Y. Song, M. Sun, S. Zhang, X. Zhang, Y. Peng, J. Liu, B. Huang, M. Huang and L. Zhang, Alleviating the Work Function of Vein-Like CoXP by Cr Doping for Enhanced Seawater Electrolysis, *Adv. Funct. Mater.*, 2023, 2214081.
- [11] C. Wang, M. Zhu, Z. Cao, P. Zhu, Y. Cao, Xu X, C. Xu, Z. Yin, Heterogeneous bimetallic sulfidesbased seawater electrolysis towards stable industrial-level large current density, *Appl. Catal. B Environ.*, 2021, **291**, 120071.
- [12] P. K. L. Tran, D. T. Tran, D. Malhotra, S. Prabhakaran, D.H. Kim. N.H. Kim and J. H. Lee, Highly Effective Freshwater and Seawater Electrolysis Enabled by Atomic Rh-Modulated Co-CoO Lateral Heterostructures, *Small*, 2021, **17**, 2103826.
- [13] T. Haq, S. A. Mansour, A. Munir and Y. Haik, Gold-Supported Gadolinium Doped CoB Amorphous Sheet: A New Benchmark Electrocatalyst for Water Oxidation with High Turnover Frequency, *Adv. Funct. Mater.*, 2020, **30**, 1910309.
- [14] G. Li, Q. Yang, J. Rao, C. Fu, S. C. Liou, G. Auffermann, Y. Sun and C. Felser, In Situ Induction of Strain in Iron Phosphide (FeP₂) Catalyst for Enhanced Hydroxide Adsorption

- and Water Oxidation, *Adv. Funct. Mater.*, 2020, **30**, 1907791.
- [15] L. Yu, H. Zhou, J. Sun, F. Qin, D. Luo, L. Xie, F. Yu, J. Bao, Y. Li, S. Chen and Z. Ren, Hierarchical Cu@CoFe layered double hydroxide core-shell nanoarchitectures as bifunctional electrocatalysts for efficient overall water splitting, *Nano Energy*, 2017, **41**, 327-336.
- [16] H. Huang, S. Zhou, C. Yu, H. Huang, J. Zhao, L. Dai and J. Qiu, Rapid and energy-efficient microwave pyrolysis for high-yield production of highly-active bifunctional electrocatalysts for water splitting, *Energy Environ. Sci.*, 2020, **13**, 545-553.
- [17] S. Hao, L. Chen, C. Yu, B. Yang, Z. Li, Y. Hou, L. Lei and X. Zhang, NiCoMo Hydroxide Nanosheet Arrays Synthesized via Chloride Corrosion for Overall Water Splitting, *ACS Energy Lett.*, 2019, **4**, 952-959.